Petroleum Science 18 (2021) 1483–1491

Contents lists available at ScienceDirect

Petroleum Science

journal homepage: www.keaipublishing.com/en/journals/petroleum-science

Original Paper

Properties, combustion behavior, and kinetic triplets of coke produced by low-temperature oxidation and pyrolysis: Implications for heavy oil in-situ combustion

Shuai Zhao [a, b, *], Wan-Fen Pu [a], Lei Su [c], Ce Shang [c], Yang Song [c], Wei Li [c], Hui-Zhuo He [c], Yi-Gang Liu [d], Zhe-Zhi Liu [d]

[a] State Key Laboratory of Oil and Gas Reservoir Geology and Exploitation, Southwest Petroleum University, Chengdu, Sichuan, 610500, China
[b] Post-Doctorate R&D Base, Southwest Petroleum University, Chengdu, Sichuan, 610500, China
[c] E&D Research Institute of Liaohe Oilfield CNPC, Panjin, Liaoning, 124000, China
[d] School of Oil and Gas Engineering, Chongqing University of Science and Technology, Chongqing, 401331, China

ARTICLE INFO

Article history:
Received 24 June 2020
Accepted 29 March 2021
Available online 17 August 2021

Edited by Yan-Hua Sun

Keywords:
Oxidized coke
Pyrolyzed coke
Heavy oil
In-situ combustion
Kinetic triplets

ABSTRACT

This work aimed at investigating the crucial factor in building and maintaining the combustion front during in-situ combustion (ISC), oxidized coke and pyrolyzed coke. The surface morphologies, elemental contents, and non-isothermal mass losses of the oxidized and pyrolyzed cokes were thoroughly examined. The results indicated that the oxidized coke could be combusted at a lower temperature compared to the pyrolyzed coke due primarily to their differences in the molecular polarity and microstructure. Kinetic triplets of coke combustion were determined using iso-conversional models and one advanced integral master plots method. The activation energy values of the oxidized and pyrolyzed cokes varied in the range of 130–153 kJ/mol and 95–120 kJ/mol, respectively. The most appropriate reaction model of combustion of the oxidized and pyrolyzed cokes followed three-dimensional diffusion model (D_3) and random nucleation and subsequent growth model (F_1), respectively. These observations assisted in building the numerical model of these two types of cokes to simulate the ISC process.

1. Introduction

With the decline of conventional oil production together with the ever-increasing energy consumption, global attention has been placed on unconventional oil resources, such as heavy oil (Kok and Gundogar, 2013; Kok et al., 2017; Zhao et al., 2015). Thermal enhanced oil recovery (EOR) strategies are the most important methods in terms of exploiting heavy oil, among which in-situ combustion (ISC) has proven to be very promising. In a successful ISC operation, after air injection and ignition, a formed combustion zone can propagate from the injection well to the production well, during which a large amount of heat yielded by combustion results in improved oil production and in-situ upgrading of heavy oil (Zhao et al., 2019b). As agreed, the main fuel provided for combustion is the coke produced by heavy oil from in-situ thermal conversion (Hascakir et al., 2013; Liu, 2018; Zhao et al. 2018b, 2019d). Therefore, the quantity and reactivity of coke directly affect the movement and sustainability of the combustion front, accordingly playing a vital influence on ISC performance.

In the reservoir conditions, coke has been found to be the primary product of two types of reactions, known as low-temperature oxidation (LTO) and pyrolysis (Alexander et al., 1962). During ISC, part of oxygen breaks through the combustion front and further reacts with the oil ahead of the combustion front, eventually generating the coke with different oxygen-containing functional groups through multistage chain reactions initiated by the free radicals (Jia et al., 2016; Li et al., 2020; Varfolomeev et al., 2016). Some scholars found that after being oxidized for 7 days at 40 MPa and 120 °C, one extra-heavy crude oil collected from the Tahe Oilfield was partially transformed into coke that was easily ignited

* Corresponding author. State Key Laboratory of Oil and Gas Reservoir Geology and Exploitation, Southwest Petroleum University, Chengdu, Sichuan, 610500, China.
E-mail address: zs77816@163.com (S. Zhao).

https://doi.org/10.1016/j.petsci.2021.08.005

at ambient temperature and pressure (Pu et al., 2015). The chemical-structural properties of the coke induced by LTO were analyzed (Xu et al., 2017). The results indicated the oxidized coke included various oxygen-containing functionalities and highly-substituted aromatic rings. Besides, the oxidized coke had highly disorder amorphous structures associated with poorly order 'onion-like' structures. The second type of coke is termed as pyrolyzed coke (Khansari et al., 2014; Murugan et al., 2010). Usually, a portion of the crude oil located in front of the combustion front without oxygen is susceptible to thermal pyrolysis as the temperature attains approximately 400 °C, during which the pyrolyzed coke is yielded due to the breakup of colloidal structure of the oil as well as subsequent aggregation and deposition of heavy fractions (Buckley, 2012; Xu et al., 2016).

In recent years, some researchers investigated the influence of coking atmosphere on the quantity and reactivity of formed coke (Cinar et al., 2011; Torregrosa-Rodrıguez et al., 2000; Xu et al., 2017). Cinar et al. (2011) reported that the coke yield in an inert atmosphere merely accounted for a quarter to a half of that in an oxidized atmosphere. The coke properties, such as color, odor, hydrogen content, and so forth, were apparently changed by LTO reactions of heavy oil if compared to those by thermal pyrolysis as claimed by Dabbous et al. (1974). In addition, the coke combustion kinetics is of great importance to the ISC numerical modeling, which is an indispensable part of the reservoir simulation. It was found by Zhang (2015) that the oxidation rate at 350 °C of the oxidized coke was at least two orders of magnitude higher than that of the pyrolyzed coke. More recently, the relation of activation energy versus conversion degree during combustion of the oxidized and pyrolyzed cokes was determined using the thermogravimetry (TG) data with multiple different heating rates and one iso-conversional model named Ozawa-Flynn-Wall (OFW). The results suggested that these two types of cokes had different values of activation energy, thus affecting the difficulty level of coke combustion. Also, it was observed that the pyrolyzed coke was more suitable as fuel serving as ISC because its activation energy reduced consecutively after combustion proceeded (Li et al., 2020). Meanwhile, a few researchers proposed some simplified reaction schemes for ISC, including combustion of the oxidized and pyrolyzed cokes (Cinar et al., 2011; Zhu et al., 2019). However, the combustion mechanisms of these two types of cokes were seldom studied, leading to the difficulties in accurately determining the reaction models of coke combustion when considering modeling the ISC process.

In this work, one heavy oil from the Xinjiang Oilfield in China was experimentally subjected to static oxidation and pyrolysis under different temperatures, followed by the coke separation. The surface morphologies, elemental contents, and non-isothermal mass losses of the oxidized and pyrolyzed cokes were then examined with the intention of disclosing the primary reason behind their differences in reactivity. Subsequently, the kinetic triplets of coke combustion were determined using two iso-conversional models and one advanced integral master plots method, by which the underlying combustion mechanisms could be well understood. This work can bring some new insights into the coke combustion mechanisms and facilitate evaluating the thermodynamic feature of combustion reactions.

2. Experimental

2.1. Materials

The heavy oil was collected from the Xinjiang Oilfield, China and its basic properties is listed in Table 1. The chemicals used herein, including toluene, heptane, ethanol, and so forth, were provided by Kelong Chemical Co., Ltd. (Chengdu, China) and used as received.

2.2. Static oxidation and pyrolysis experiments

The simplified schematic diagram of the static experiments is illustrated in Fig. 1. The operating procedures were described as follows. (1) A given volume of crude oil (~60 mL) was loaded into the reactor. (2) The sealed reactor was pressurized to 15 MPa using air in the oxidation runs at a given temperature, while nitrogen was injected in the pyrolysis runs. (3) The reaction products were taken out after six days. The targeted reservoir was exploited by steam injection, during which the temperatures of different reservoir zones ranged from 40 to 200 °C. At present the ISC technique is being applied to this reservoir after steam injection. For this reason, we chose 40, 80, 120, 160, and 200 °C as the environment temperature in the oxidation runs. Three temperature levels (350, 400, and 450 °C) were selected as the experimental temperature in the pyrolysis runs according to the previous investigations (Li et al., 2020; Xu et al., 2016).

2.3. Coke separation

The oxidation and pyrolysis products were washed by toluene to separate the coke samples, followed by drying in a nitrogen atmosphere at 100 °C. The obtained coke samples were used for the subsequent analyses.

2.4. Scanning electron microscopy (SEM) and energy-dispersive X-ray spectroscopy (EDS)

A scanning electron microscopy (SEM) coupled with energy-dispersive X-ray spectroscopy (EDS) (ZEISS EVO MA15, Carl Zeiss Ltd.) was employed to examine the microscopic structures and elemental contents of the coke samples.

2.5. Thermogravimetry (TG)

The combustion characteristics of the coke samples were investigated using NETZSCH STA 449F3 PC/PG equipped with a TG module. Before the tests, the thermo-analysis system should be calibrated, referring to the method illustrated in the previous publications (Li et al., 2017b; Zhao et al., 2019a). The operational procedures included placing a certain amount of the sample (~5 mg), setting the air flow rate (50 mL/min), and heating rates (5, 10, and 15 °C/min), then initiating the test.

3. Results and discussion

3.1. Coke content

The influences of the coking atmosphere and temperature on the coke deposition were analyzed in this section. The experiments conducted in the air and nitrogen atmospheres were named as the LTO and pyrolysis runs, respectively. Fig. 2 shows the amount of coke yielded in the LTO and pyrolysis runs. In the case of the LTO runs, there was some oxidized coke being separated only as the temperature was increased to 200 °C. With regard to the pyrolysis runs, the pyrolysis products at 350 and 400 °C remained the liquid phase, whereas those at 450 °C became the liquid oil and black solid matter as shown in Fig. 3. The viscosity of this liquid oil at 50 °C was only 6.8 mPa s, far less than that of the crude oil. This fact indicated that with the advancement of combustion front, the high temperature not only activated the oil through decreasing its viscosity but also achieved in-situ upgrading of the oil. Besides, the obtained black solid matter was subjected to the coke separation according

Table 1
SARA fractions and basic properties of heavy crude oil.

Viscosity, mPa·s @50 °C	SARA fractions, wt%				Element analysis, wt%				
	Saturates	Aromatics	Resins	Asphaltenes	C	H	O	N	S
610	50.69	30.58	14.81	3.92	80.70	13.20	2.76	0.72	0.91

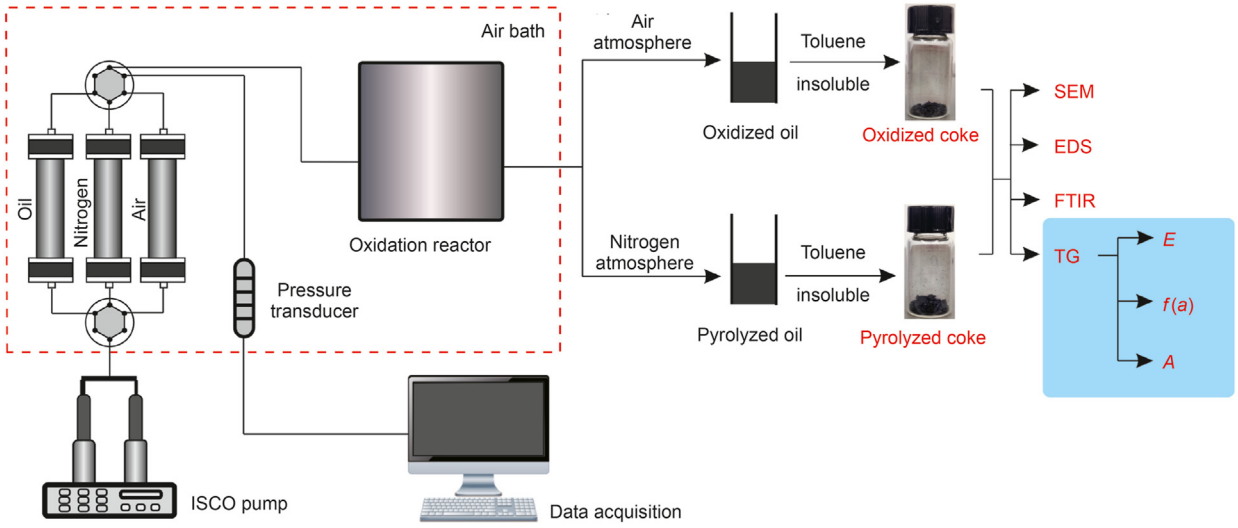

Fig. 1. Workflow of this work.

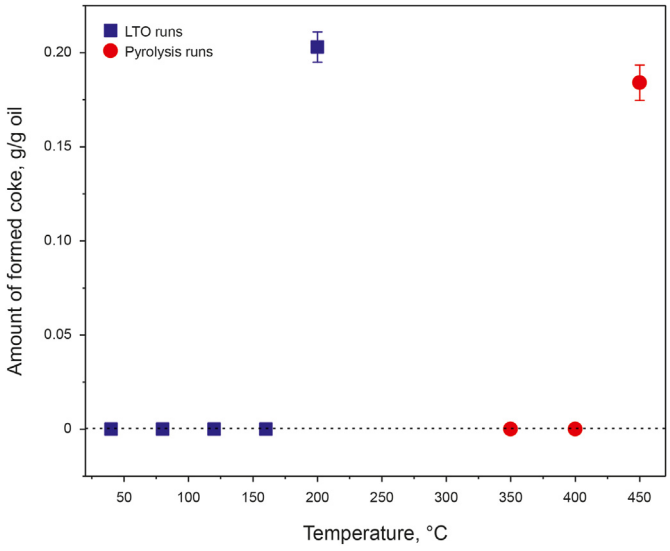

Fig. 2. Amount of coke formed in the LTO and pyrolysis runs.

to the method described in Section 2.3. Eventually, this matter was found to be almost insoluble in toluene, which meant it was the pyrolyzed coke. In addition, the above results also revealed that the coke was formed more readily in an air atmosphere relative to a nitrogen atmosphere, where was predominantly related to different coking mechanisms (Cinar et al., 2011; Xu et al., 2016). In the LTO process, oxygen atoms attack active hydrogen present in polar molecules to produce a series of oxygenated groups, such as carboxyl group and ester group. Part of these groups are inclined to condense and thus form heavier compositions, accordingly destroying the stability of colloidal system of crude oil and causing the coke deposition. Regarding the pyrolysis runs, the colloidal structure of crude oil is broken due to the pyrolysis of the oil components. This consequently makes the asphaltene cores dissolved in maltenes exceed the solubility limit and precipitate to yield coke (Wiehe, 1993). In summary, the LTO reactions intensified the instability of colloidal structure of crude oil, so the coke formation was advanced.

3.2. Morphology observations

In this section, SEM was used to visually determine the surface morphologies of the oxidized and pyrolyzed cokes. Fig. 4 shows the SEM images of the oxidized coke at two magnifications. It was seen from Fig. 4(a) that numerous particles with different sizes existed on the surface of oxidized coke, predominantly caused by the condensation reactions of oxygen-containing derivatives. The surface of coke was found to have a lot of pores at a higher magnification as exhibited in Fig. 4(b). The interpretation of this finding might be that some hydrocarbons were evaporated from the liquid phase during LTO as reported by Khansari et al. (2012) and Yuan et al. (2018). The porous formation notably increased the contact area between coke and oxygen and thus promoted coke combustion. The pyrolyzed coke was larger in size than the oxidized coke as observed from Figs. 4(a) and 5(a), suggesting stronger aggregation and deposition of heavy fractions in the pyrolysis run. The apparent textural differences of the oxidized and pyrolyzed cokes could be clearly observed from Figs. 4(b) and 5(b). The surface of pyrolyzed coke was covered by plenty of ball-like structures, which might be carbon aggregation resulting from the polycondensation effect.

3.3. Elemental analysis

The EDS spectra of the oxidized and pyrolyzed cokes are exhibited in Fig. 6, by which the relative elemental contents could

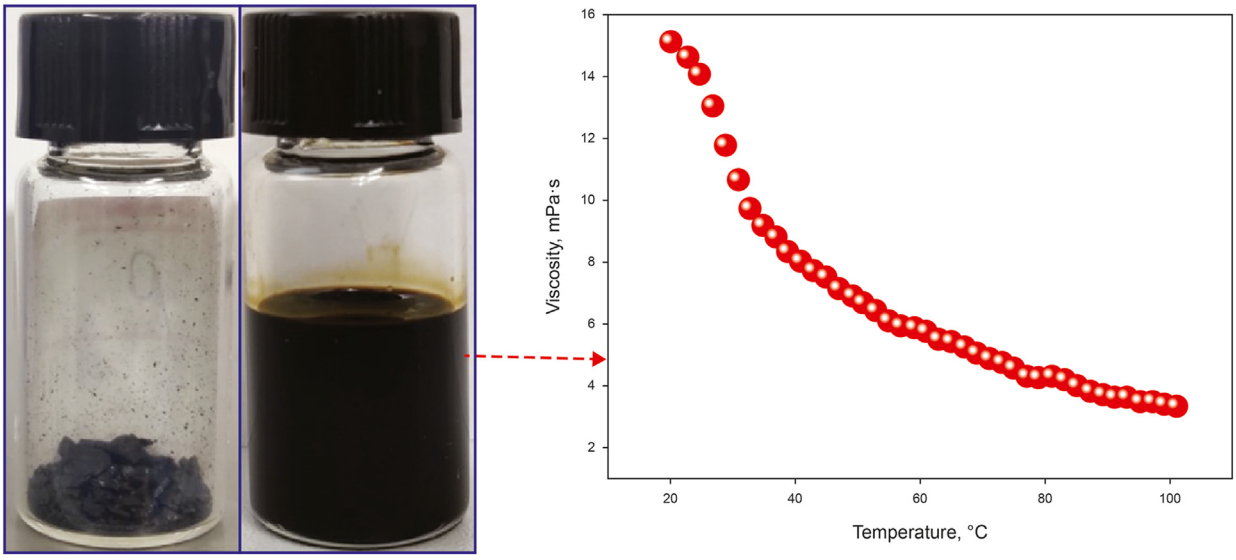

Fig. 3. Pyrolyzed products of heavy crude oil at 450 °C and the dependence of viscosity of the liquid oil on temperature.

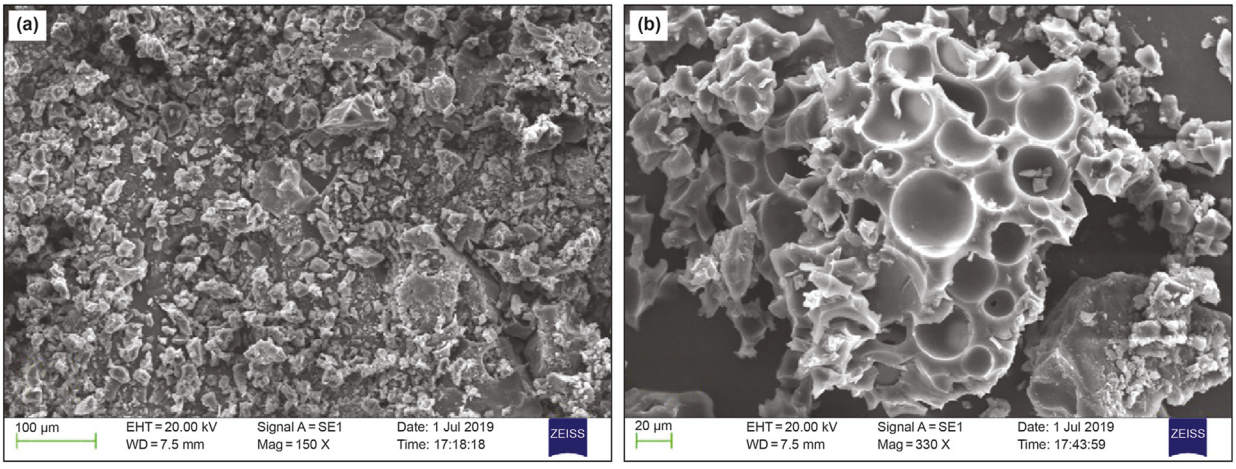

Fig. 4. SEM images of oxidized coke.

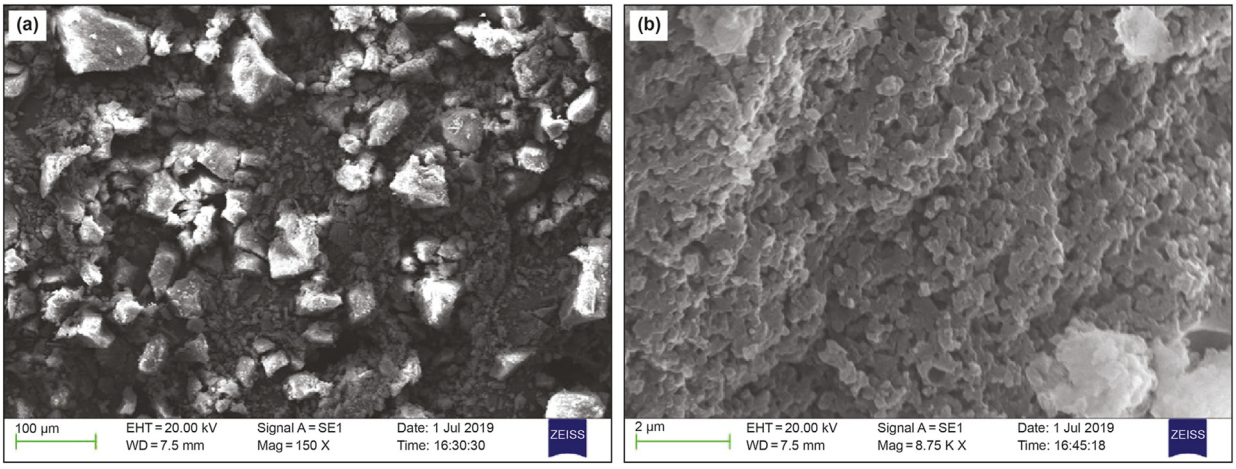

Fig. 5. SEM images of pyrolyzed coke.

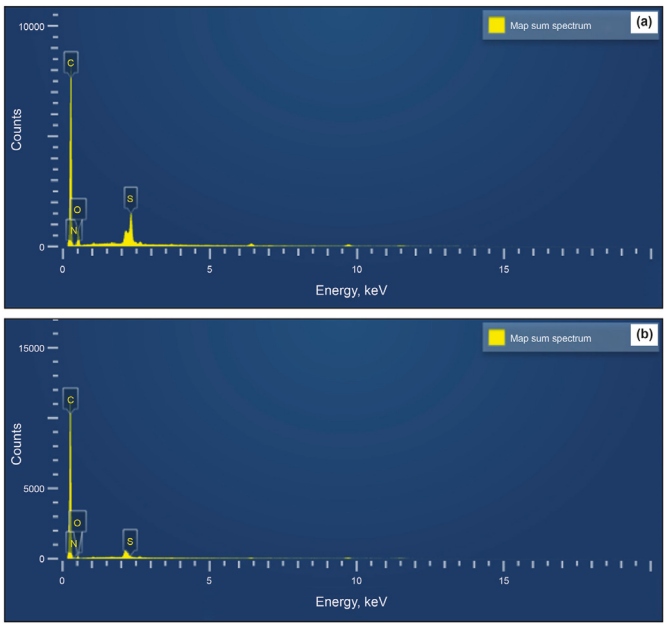

Fig. 6. EDS spectra of (**a**) oxidized coke and (**b**) pyrolyzed coke.

Table 2
Elemental contents of the coke samples.

Sample	Elemental content, %				C/O atomic ratio
	C	N	O	S	
Oxidized coke	83.20	0.08	8.99	7.72	12.34
Pyrolyzed coke	96.11	0.97	2.37	0.55	54.07

be obtained (given in Table 2). As anticipated, the oxidized coke had a higher relative content of O relative to the pyrolyzed coke because of the oxygen addition reactions during LTO. This was also revealed by the O/C atomic ratio as presented in the last column of Table 2. Interestingly, it was observed that the relative content of S of the oxidized coke accounted for 7.72%, much higher than that of the pyrolyzed coke (0.55%). It is widely acknowledged that S is mainly contained in heavy components, especially asphaltenes. Oxygen atoms are more likely to react with macromolecules rich in polar groups, such as asphaltenes, to yield oxygenated derivatives according to the free radicals theories (Freitag, 2016; Zhao et al., 2019c). As described in Section 3.1, these oxygenated derivatives readily condensed and became the precursors for coke generation. Thus, the formed coke had most of S present in the oil sample. The C–S bond could be ruptured at temperatures above approximately 380 °C (Wei et al., 2018), so part of C–S bonds contained in heavy components were ruptured during the pyrolysis process. This accordingly resulted in the formation of some light components containing S, which were easily evaporated into the gas phase. With these points in mind, it could be well understood why the pyrolyzed coke possessed obviously lower relative content of S compared to the oxidized coke.

3.4. TG analysis

The TG technique was employed to examine the combustion characteristics of the two cokes. Fig. 7 shows the non-isothermal TG curves of the coke samples at 5, 10, and 15 °C/min. Usually, three distinct mass loss regions, named LTO, fuel deposition, and high-temperature oxidation, could be identified from the non-isothermal TG/DTG profiles of heavy oils (Pu et al., 2015; Yuan et al., 2018; Zhao et al., 2018b). However, only one distinct mass loss region appeared during the whole heating process of the two cokes, which was supposed to be the combustion region. Table 3 summarizes the TG/DTG characteristic parameters in the combustion region. It was apparent that the temperature interval of combustion was shifted to higher temperature ranges with the elevated heating rate, as a result of the more drastic thermal effect as claimed by Mothé and Miranda (2013).

The TG/DTG curves of the coke samples at 10 °C/min are presented in Fig. 8. To give a clear statement, the data at 10 °C/min would be used as a reference when it came to the analysis associated with the TG data including temperature and mass loss. The combustion regions of the oxidized and pyrolyzed cokes fell into the temperature ranges of 295–526 °C and 336–629 °C, respectively. The mass losses at the combustion stage for the oxidized and pyrolyzed cokes accounted for 90.7% and 95.9%, respectively. This result indicated that the majority of the two cokes were consumed by combustion during the heating process. Also, it was found that the combustion process of the oxidized coke was more complicated than that of the pyrolyzed coke, suggested by the fluctuating DTG curves shown in Fig. 8. Simultaneously, it was worth noting that the onset temperature of oxidized coke combustion was 41 °C lower than that of pyrolyzed coke combustion (see Table 3). This fact gave a hint that the oxidized coke was more conducive to establishing the combustion front, which was believed to be largely related to the following two aspects. First, the oxidized coke had more oxygen-containing functionalities compared to the pyrolyzed coke as we previously stated, making the oxidized coke exhibit stronger polarity and thus increase the oxidation rate. Second, the porous structure of the oxidized coke could provide larger surface area in comparison with the ball-like structure of the pyrolyzed coke as viewed from Figs. 4(b) and 5(b), which accordingly promoted the combustion reactions.

3.5. Combustion kinetic triplets

3.5.1. Estimation of the activation energy

Thermal analysis is widely implemented to determine the kinetic parameters in varying temperature regions. In this section, two classical iso-conversional models, i.e., Friedman and Ozawa-Flynn-Wall (OFW), were used to obtain the dependence of activation energy upon conversion degree during coke combustion. The final forms of the Friedman and OFW models are described by Eqs. (1) and (2), respectively (Montoya et al., 2016; Müsellim et al., 2018; Vyazovkin et al., 2011; Yao et al., 2017; Zhao et al., 2018a).

$$\ln\left(\beta_i(\mathrm{d}\alpha/\mathrm{d}T)_{\alpha,i}\right) = \ln A + \ln f(\alpha) - \frac{E_\alpha}{RT_{\alpha,i}} \tag{1}$$

$$\ln(\beta) = \ln\left(\frac{AE}{Rg(\alpha)}\right) - 5.331 - 1.052\frac{E}{RT} \tag{2}$$

where α can be expressed as:

$$\alpha = \frac{m_0 - m_t}{m_0 - m_\infty} \tag{3}$$

where α is the conversion degree, E is the activation energy, A is the frequency factor, β is the heating rate, T is the absolute temperature, R is the universal gas constant, m_t is the mass percentage of the sample at reaction time t, and m_0 and m_∞ are the initial and ending mass percentage of the sample, respectively. The value of E can be determined when plotting the regression lines of $\ln(\beta/(\mathrm{d}\alpha/\mathrm{d}T))$ against $1/T$ for Friedman and $\ln(\beta)$ against $1/T$ for OFW.

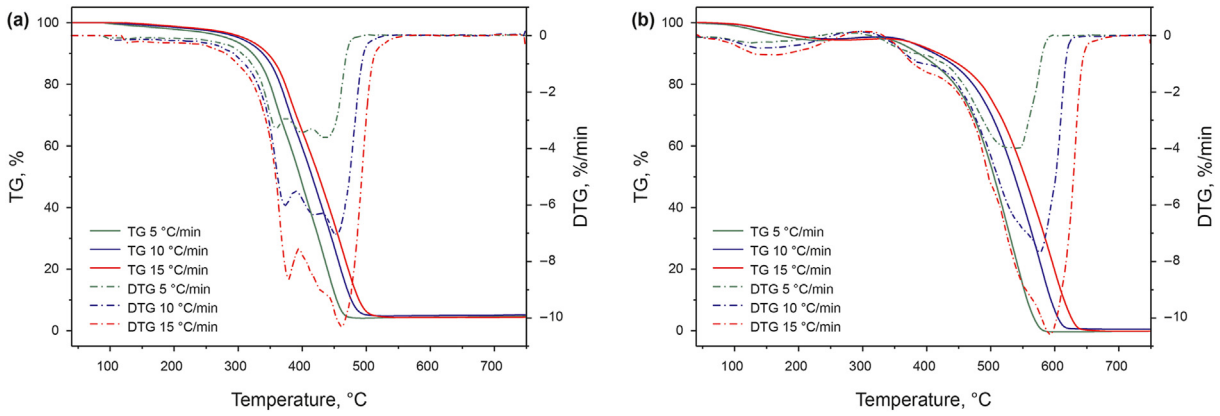

Fig. 7. TG/DTG curves of (**a**) oxidized coke and (**b**) pyrolyzed coke at different heating rates.

Table 3
TG/DTG reaction regions, peak temperatures and mass losses of the coke samples.

Sample	Heating rate, °C/min	Combustion stage			
		Onset temperature, °C/min	Ending temperature, °C/min	Peak temperature, °C	Mass loss, %
Oxidized coke	5	286	497	360//399/436	90.4
	10	295	526	373/419/450	90.7
	15	314	554	378/462	90.6
Pyrolyzed coke	5	325	594	543	95.8
	10	336	629	577	95.9
	15	348	670	592	95.7

Fig. S1 shows α as a function of T during combustion of the coke samples. Fig. 9 presents the relation of E with error bar versus α, and Table S1 in the Electrical Supplementary Material lists the values of E at α = 0.2–0.8. Even though Friedman and OFW had different theoretical basis (Vyazovkin et al., 2011), these two isoconversional models gave close kinetic parameters with small error bars, validating the high quality of the TG data obtained. The values of E of the oxidized coke changed in the range of 130–153 kJ/mol, while those of the pyrolyzed coke varied in the range of 95–120 kJ/mol. This result meant that the oxidized coke possessed higher activation energy than the pyrolyzed coke during the entire combustion process. As shown in Fig. S1(a), the corresponding temperatures at α of 0.2 and 0.8 were 364 and 453 °C, respectively.

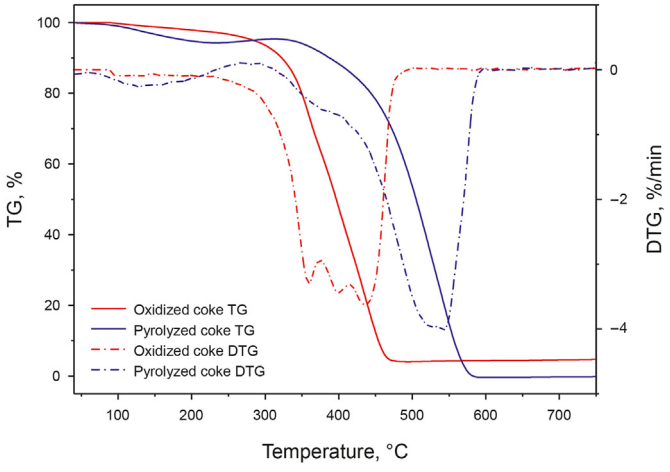

Fig. 8. Comparison of TG/DTG curves of oxidized coke and pyrolyzed coke at the heating rate of 10 °C/min.

Multiple DTG peaks of the oxidized coke appeared within the temperature range of 364–453 °C as seen from Fig. 8. It was believed that the primary reactions of the oxidized coke taking place between 364 and 453 °C included both coke combustion (exothermic effect) and coke thermo-oxidative cracking (endothermic effect). These two effects influenced the mass loss rate simultaneously, which thus caused the obvious fluctuations of DTG curves as mentioned in Section 3.4. In the case of the pyrolyzed coke, as indicated in Fig. S1(b), α of 0.2–0.8 corresponded to the temperature range of 472–579 °C. Quite a few investigations confirmed that the only one main reaction for formed coke in this temperature range was combustion (Hascakir et al., 2013; Li et al., 2017a; Zhao et al., 2021; Zheng et al., 2018). Therefore, for the oxidized coke, E was mainly used to initiate combustion and thermo-oxidative cracking simultaneously; regarding the pyrolyzed coke, E was mainly used to commence combustion. This could be partially explained why the pyrolyzed coke had lower activation energy than the oxidized coke. From the above investigations, it was believed that the pyrolyzed coke contributed more to the stable movement of combustion front relative to the oxidized coke.

3.5.2. Estimation of the reaction mechanism

The reaction mechanism involved during coke combustion was determined using the integral master plots method (Sharma et al. 2018, 2019). The integral form of the reaction can be described as Eq. (4) according to this method.

$$g(\alpha) \equiv \int_0^{\alpha} \frac{\mathrm{d}\alpha}{f(\alpha)} = \int_{T_0}^{T} \frac{A}{\beta} \exp\left(-\frac{E}{RT}\right) \mathrm{d}T \approx \int_0^{T} \frac{A}{\beta} \exp\left(-\frac{E}{RT}\right) \mathrm{d}T = \frac{AE}{\beta R} P(u) \tag{4}$$

where $f(\alpha)$ is the reaction model, $g(\alpha)$ is the integral form of reaction

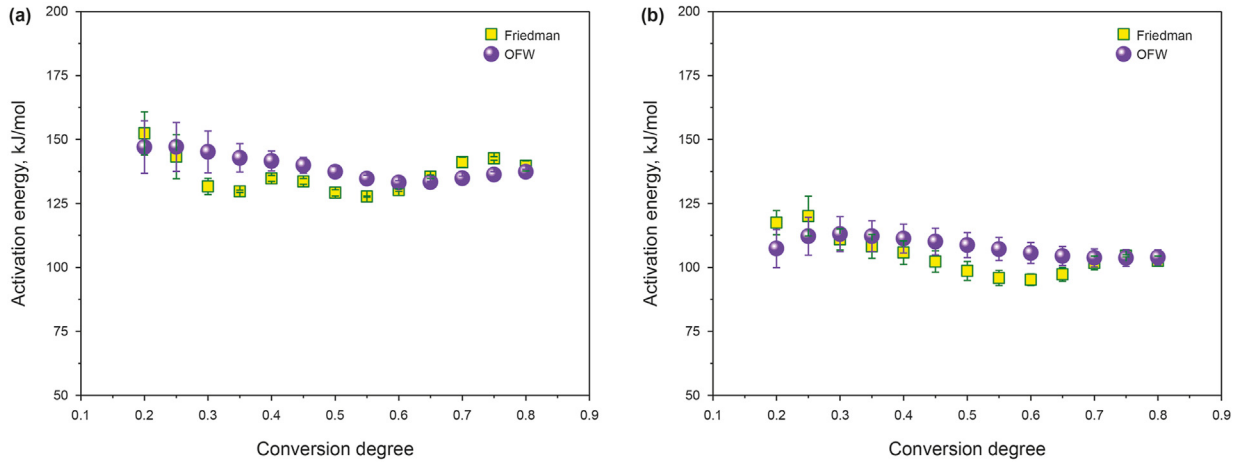

Fig. 9. Activation energy as a function of conversion degree for combustion of (**a**) oxidized coke and (**b**) pyrolyzed coke.

Table 4
Mathematical expressions of functions, $f(\alpha)$ and $g(\alpha)$, for different classical reaction models.

No.1	Reaction model	Code	$f(\alpha)$	$g(\alpha)$
1	Power law (Acceleratory rate equations)	P_2	$2\alpha^{1/2}$	$\alpha^{1/2}$
2		P_3	$3\alpha^{2/3}$	$\alpha^{1/3}$
3		P_4	$4\alpha^{3/4}$	$\alpha^{1/4}$
4	Avrami–Erofeev (Sigmoidal rate equations)	A_2	$2(1-\alpha)[-\ln(1-\alpha)]^{1/2}$	$[-\ln(1-\alpha)]^{1/2}$
5		A_3	$3(1-\alpha)[-\ln(1-\alpha)]^{2/3}$	$[-\ln(1-\alpha)]^{1/3}$
6		A_4	$4(1-\alpha)[-\ln(1-\alpha)]^{3/4}$	$[-\ln(1-\alpha)]^{1/4}$
7	One-dimensional diffusion	D_1	$(1/2)\alpha^{-1}$	α^2
8	Two-dimensional diffusion	D_2	$[-\ln(1-\alpha)]^{-1}$	$\alpha+(1-\alpha)\ln(1-\alpha)$
9	Three-dimensional diffusion	D_3	$[(3/2)(1-\alpha)^{2/3}][1-(1-\alpha)^{1/3}]^{-1}$	$(1-(1-\alpha)^{1/3})^2$
10	Four-dimensional diffusion	D_4	$(3/2)[(1-\alpha)^{-1/3}-1]^{-1}$	$1-2\alpha/3-(1-\alpha)^{2/3}$
11	Phase boundary controlled reaction (Deceleratory rate equations)	R_1	Constant	α
12		R_2	$2(1-\alpha)^{1/2}$	$1-(1-\alpha)^{1/2}$
13		R_3	$3(1-\alpha)^{2/3}$	$1-(1-\alpha)^{1/3}$
14	First order	F_1	$1-\alpha$	$-\ln(1-\alpha)$
15	Second order	F_2	$(1-\alpha)^2$	$(1-\alpha)^{-1}-1$
16	Third order	F_3	$(1-\alpha)^3$	$[(1-\alpha)^{-2}-1]/2$

model, $P(u)$ is the temperature integral, and $u = E/RT$.

Furthermore, to estimate the reaction model, Eq. (5) can be described as:

$$\frac{g(\alpha)}{g(0.5)} = \frac{P(u)}{P(0.5)} \tag{5}$$

$P(u)$ can be expressed as (Sharma et al., 2018) :

$$P(u) \cong \frac{\exp(-1.0008u - 0.312)}{u^{0.92}} \tag{6}$$

The theoretical master profiles corresponded to varying reaction mechanisms summarized in Table 4 (Karimian et al., 2017; Shahcheraghi et al., 2016; Vyazovkin et al., 2011), and were determined by plotting $g(\alpha)/g(0.5)$ versus a. The experimental profiles were obtained by plotting $P(u)/P(0.5)$ versus α. Comparison between the theoretical master profiles and experimental profiles assisted in selecting the proper reaction model.

Fig. 10 presents the theoretical master profiles and the experimental profiles for combustion of the coke samples. As known from Fig. 10(a), the most appropriate reaction model of the oxidized coke was the D_3 model featured with three-dimensional diffusion and spherical symmetry. This finding unraveled that the three-dimensional diffusion between the oxidized coke and oxygen was the rate-determining mechanism to dominate combustion. With regard to the pyrolyzed coke, it was found that the F_1 model was the most suitable function, disclosing that the random nucleation and subsequent growth was the most probable mechanism. In terms of α versus reaction time, D_3 and F_1 belonged to the decelerating and sigmoidal reaction models, respectively. This indicated that the reaction rate reached the maximum value at the initial stage and decreased continuously with the increase in α during oxidized coke combustion, whereas the reaction rate firstly increased and then decreased as pyrolyzed coke combustion progressed. The above findings further reflected that the oxidized coke contributed more to the establishment of the combustion front at the initial stage of ignition, while the pyrolyzed coke contributed more to the subsequent movement of the combustion front, as stated in Sections 3.4 and 3.5.1.

3.5.3. Estimation of the frequency factor

The value of A was estimated by substituting E and reaction model in Eq. (4). In the case of oxidized coke combustion, Eq. (4) can be described as:

$$g\left(\alpha\right) = \frac{AE}{\beta R} P\left(u\right) = 1-\alpha\Big)\Big(1-\alpha\Big)(1-\alpha)^{1/3}\Big)^2 \tag{7}$$

Regarding pyrolyzed coke combustion, Eq. (4) can be written as:

$$g(\alpha) = \frac{AE}{\beta R} P(u) = -\ln(1-\alpha) \tag{8}$$

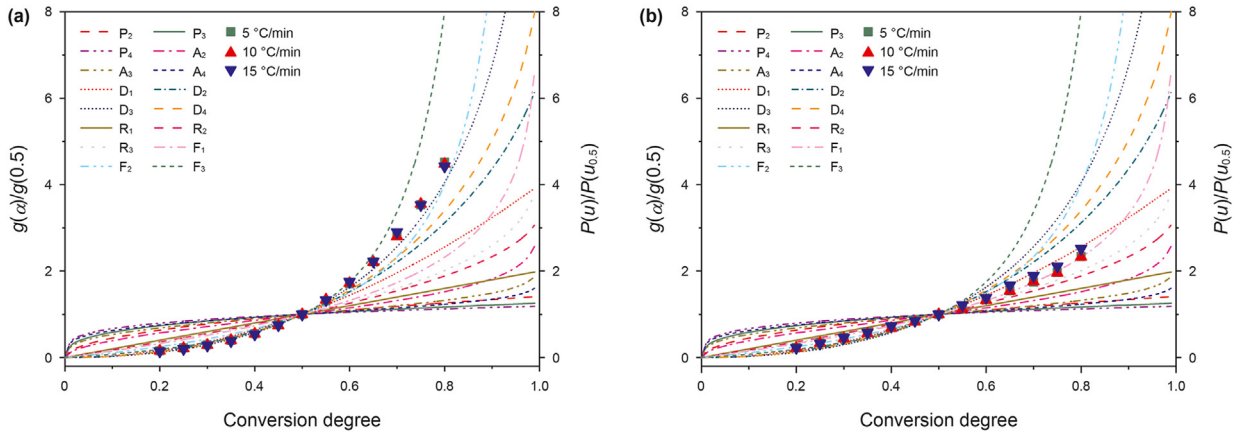

Fig. 10. Comparison of the theoretical master curves with the experimental curves determined from the integral master-plots method for combustion of (**a**) oxidized coke and (**b**) pyrolyzed cok.

Table 5
Kinetic triplets for combustion of the coke samples.

Sample	Heating rate, °C/min	Average E, kJ/mol		A, s^{-1}	$f(\alpha)$	R^2
		Friedman	OFW			
Oxidized coke	5	136.3	139.3	2.436E7	$[(3/2)(1-\alpha)^{2/3}][1-(1-\alpha)^{1/3}]^{-1}$	0.999
	10			2.474E7		0.999
	15			2.483E7		0.999
Pyrolyzed coke	5	104.7	108.0	8.384E4	$1-\alpha$	0.998
	10			8.142E4		0.998
	15			8.283E4		0.998

The value of A was determined for the oxidized coke at 10 °C/min when plotting the regression line of $(1-(1-\alpha)^{1/3})^2$ against $EP(u)/(\beta R)$, as shown in Fig. S2(a). Similarly, the value of A for the pyrolyzed coke at 10 °C/min was determined (see Fig. S2(b)). In this way, the values of A at 5 and 15 °C were obtained (given in Figs. S3 and S4). Table 5 is presented to show the kinetic triplets for combustion of the coke samples. The oxidized coke had higher molecular collision frequency during combustion, demonstrated by the considerably higher frequency factor relative to the pyrolyzed coke at any heating rate. The basic kinetic equation was easily deconvolved after the kinetic triplets were obtained, which assisted in determining the reaction schemes of these two types of cokes for the modeling of the ISC process.

4. Conclusions

Due to the significance of coke in the combustion front during ISC, this work thoroughly studied the properties, combustion behavior, and kinetic triplets of the oxidized and pyrolyzed cokes. The primary conclusions could be summarized as follows.

(1) In the LTO runs, the heavy oil could be partially transformed into coke as the temperature increased to 200 °C. In the pyrolysis runs, the heavy oil was directly pyrolyzed into light oil and coke at 450 °C.
(2) The oxidized coke was more conducive to establishing the combustion front at the initial stage of ignition, suggested by the obviously lower onset temperature of combustion compared to the pyrolyzed coke.
(3) The pyrolyzed coke contributed more to the stable movement of combustion front than the oxidized coke, as revealed by the values of activation energy.
(4) The three-dimensional diffusion (D_3) between the coke and oxygen was the rate-determining mechanism to dominate oxidized coke combustion. The random nucleation and subsequent growth mechanism (F_1) was the most probable mechanism for pyrolyzed coke combustion.

Acknowledgements

This work was supported by Chinese Postdoctoral Science Foundation (2021M692696), the National Science and Technology Project (2016ZX05058-003-017), and Sichuan Science and Technology Program (2021YFH0081).

Appendix A. Supplementary data

Supplementary data to this article can be found online at https://doi.org/10.1016/j.petsci.2021.08.005.

References

Alexander, J.D., Martin, W.L., Dew, J.N., 1962. Factors affecting fuel availability and composition during in situ combustion. J. Petrol. Technol. 14 (10), 1154–1164. https://doi.org/10.2118/296-PA.
Buckley, J.S., 2012. Asphaltene deposition. Energy Fuels 26 (7), 4086–4090. https://doi.org/10.1021/ef300268s.
Cinar, M., Castanier, L.M., Kovscek, A.R., 2011. Combustion kinetics of heavy oils in porous media. Energy Fuels 25 (10), 4438–4451. https://doi.org/10.1021/ef200680t.
Dabbous, M.K., Fulton, P.F., 1974. Low-temperature-oxidation reaction kinetics and effects on the in-situ combustion process. SPE J. 14 (3), 253–262. https://doi.org/10.2118/4143-PA.
Freitag, N.P., 2016. Chemical reaction mechanisms that govern oxidation rates during in-situ combustion and high-pressure air injection. SPE Reservoir Eval. Eng. 19, 645–654. https://doi.org/10.2118/170162-PA.
Hascakir, B., Ross, C., Castanier, L.M., Kovscek, A., 2013. Fuel formation and conversion during in-situ combustion of crude oil. SPE J. 18 (6), 1217–1228. https://doi.org/10.2118/146867-PA.

Jia, H., Liu, P.G., Pu, W.F., Ma, X.P., Zhang, J., 2016. In situ catalytic upgrading of heavy crude oil through low-temperature oxidation. Petrol. Sci. 13, 476–488. https://doi.org/10.1007/s12182-016-0113-6.
Karimian, M., Schaffie, M., Fazaelipoor, M.H., 2017. Estimation of the kinetic triplet for in-situ combustion of crude oil in the presence of limestone matrix. Fuel 209, 203–210. https://doi.org/10.1016/j.fuel.2017.07.098.
Khansari, Z., Gates, I.D., Mahinpey, N., 2012. Detailed study of low-temperature oxidation of an Alaska heavy oil. Energy Fuels 26 (3), 1592–7159. https://doi.org/10.1021/ef201828p.
Khansari, Z., Gates, I.D., Mahinpey, N., 2014. Low-temperature oxidation of Lloydminster heavy oil: kinetic study and product sequence estimation. Fuel 115 (1), 534–538. https://doi.org/10.1016/j.fuel.2013.07.071.
Kok, M.V., Gundogar, A.S., 2013. DSC study on combustion and pyrolysis behaviors of Turkish crude oils. Fuel Process. Technol. 116 (6), 110–115. https://doi.org/10.1016/j.fuproc.2013.05.001.
Kok, M.V., Varfolomeev, M.A., Nurgaliev, D.K., 2017. Thermal characterization of crude oils in the presence of limestone matrix by TGA-DTG-FTIR. J. Petrol. Sci. Eng. 154, 495–501. https://doi.org/10.1016/j.petrol.2017.02.001.
Li, Y.B., Chen, Y., Pu, W.F., Gao, H., Bai, B., 2017a. Experimental investigation into the oxidative characteristics of Tahe heavy crude oil. Fuel 209, 194–202. https://doi.org/10.1016/j.fuel.2017.07.029.
Li, Y.B., Chen, Y.F., Pu, W.F., Dong, H., Gao, H., Jin, F.Y., et al., 2017b. Low temperature oxidation characteristics analysis of ultra-heavy oil by thermal methods. J. Ind. Eng. Chem. 48, 249–258. https://doi.org/10.1016/j.jiec.2017.01.017.
Li, Y.B., Luo, C., Lin, X., Li, K., Xiao, Z.R., Wang, Z.Q., et al., 2020. Characteristics and properties of coke formed by low-temperature oxidation and thermal pyrolysis during in situ combustion. Ind. Eng. Chem. Res. 59 (5), 2171–2180. https://doi.org/10.1021/acs.iecr.9b05635.
Liu, D., Chen, L.J., Chen, L., Zheng, R.N., Song, Q., Cai, G., 2018. Influence of conversion conditions on heavy-oil coking during in situ combustion process. Energy Fuels 32, 4823–4832. https://doi.org/10.1021/acs.energyfuels.8b00098.
Montoya, T., Argel, B.L., Nassar, N.N., Franco, C.A., Cortés, F.B., 2016. Kinetics and mechanisms of the catalytic thermal cracking of asphaltenes adsorbed on supported nanoparticles. Petrol. Sci. 13 (3), 561–571. https://doi.org/10.1007/s12182-016-0100-y.
Mothé, C.G., Miranda, I.C.D., 2013. Study of kinetic parameters of thermal decomposition of bagasse and sugarcane straw using Friedman and Ozawa–Flynn–-Wall iso-conversional methods. J. Therm. Anal. Calorim. 113 (2), 497–505. https://doi.org/10.1007/s10973-013-3163-7.
Murugan, P., Mahinpey, N., Mani, T., Asghari, K., 2010. Effect of low-temperature oxidation on the pyrolysis and combustion of whole oil. Energy 35 (5), 2317–2322. https://doi.org/10.1016/j.energy.2010.02.022.
Müsellim, E., Tahir, M.H., Ahmad, M.S., Ceylan, S., 2018. Thermokinetic and TG/DSC-FTIR study of pea waste biomass pyrolysis. Appl. Therm. Eng. 137, 54–61. https://doi.org/10.1016/j.applthermaleng.2018.03.050.
Pu, W.F., Yuan, C.D., Jin, F.Y., Wang, L., Qian, Z., Li, Y.B., et al., 2015. Low-temperature oxidation and characterization of heavy oil via thermal analysis. Energy Fuels 29 (2), 1151–1159. https://doi.org/10.1021/ef502135e.
Shahcheraghi, S.H., Khayati, G.R., Ranjbar, M., 2016. An advanced reaction model determination methodology in solid-state kinetics based on Arrhenius parameters variation. J. Therm. Anal. Calorim. 123 (1), 221–229. https://doi.org/10.1007/s10973-016-5473-z.
Sharma, P., Kaur, T., Pandey, O.P., 2018. In situ single-step reduction and silicidation of MoO_3 to form $MoSi_2$. J. Am. Ceram. Soc. 102, 1522–1534. https://doi.org/10.1111/jace.15994.
Sharma, P., Pandey, O., Diwan, P., 2019. Non-isothermal kinetics of pseudo-components of waste biomass. Fuel 253, 1149–1161. https://doi.org/10.1016/j.fuel.2019.05.093.
Torregrosa-Rodrıguez, P., Martınez-Escandell, M., Rodrıguez-Reinoso, F., Marsh, H., De Salazar, C.G., Palazón, E.R., 2000. Pyrolysis of petroleum residues: II. Chemistry of pyrolysis. Carbon 38 (4), 535–546. https://doi.org/10.1016/S0008-6223(99)00133-5.
Varfolomeev, M.A., Galukhin, A., Nurgaliev, D.K., Kok, M.V., 2016. Thermal decomposition of Tatarstan Ashal'cha heavy crude oil and its SARA fractions. Fuel 186, 122–127. https://doi.org/10.1016/j.fuel.2016.08.042.
Vyazovkin, S., Burnham, A.K., Criado, J.M., Pérez-Maqueda, L.A., Popescu, C., Sbirrazzuoli, N., 2011. ICTAC Kinetics Committee recommendations for performing kinetic computations on thermal analysis data. Thermochim. Acta 520 (1), 1–19. https://doi.org/10.1016/j.tca.2011.03.034.
Wei, B., Zou, P., Zhang, X., Xu, X.G., Wood, C., Li, Y.B., 2018. Investigations of structure-property-thermal degradation kinetics alterations of Tahe asphaltenes caused by low temperature oxidation. Energy Fuels 32, 1506–1514. https://doi.org/10.1021/acs.energyfuels.7b03565.
Wiehe, I.A., 1993. A phase-separation kinetic model for coke formation. Ind. Eng. Chem. Res. 32 (11), 2447–2454. https://doi.org/10.1021/ie00023a001.
Xu, Q., Hang, J., Cheng, Z., Tang, W., Ran, X., Jia, H., et al., 2016. Coke formation and coupled effects on pore structure and permeability change during crude oil in situ combustion. Energy Fuels 30 (2), 933–942. https://doi.org/10.1021/acs.energyfuels.5b02600.
Xu, Q., Liu, Z., Jiang, H., Zhang, Q., Zan, C., Ma, D., et al., 2017. Chemical-structural properties of the coke produced by low temperature oxidation reactions during crude oil in-situ combustion. Fuel 207, 179–188. https://doi.org/10.1016/j.fuel.2017.06.026.
Yao, Z., Ma, X., Wang, Z., Chen, L., 2017. Characteristics of co-combustion and kinetic study on hydrochar with oil shale: a thermogravimetric analysis. Appl. Therm. Eng. 110, 1420–1427. https://doi.org/10.1016/j.applthermaleng.2016.09.063.
Yuan, C., Emelianov, D.A., Varfolomeev, M.A., 2018. Oxidation behavior and kinetics of light, medium, and heavy crude oils characterized by thermogravimetry coupled with Fourier transform infrared spectroscopy. Energy Fuels 32 (4), 5571–5580. https://doi.org/10.1021/acs.energyfuels.8b00428.
Zhang, Y., 2015. Analysis of the Coke Physical and Chemical Properties during Crude Oil In-Situ Combustion Process. Master Thesis. Tsinghua University, Beijing (in Chinese).
Zhao, R.B., Chen, Y.X., Huan, R.P., Castanier, L.M., Kovscek, A.R., 2015. An experimental investigation of the in-situ combustion behavior of Karamay crude oil. J. Petrol. Sci. Eng. 127, 82–92. https://doi.org/10.1016/j.petrol.2015.01.005.
Zhao, S., Pu, W., Varfolomeev, M.A., Yuan, C., Pan, J., Wang, R., et al., 2018a. Low-temperature oxidation of light and heavy oils via thermal analysis: kinetic analysis and temperature zone division. J. Petrol. Sci. Eng. 168, 246–255. https://doi.org/10.1016/j.petrol.2018.05.031.
Zhao, S., Pu, W.F., Varfolomeev, M.A., Yuan, C.D., Zhang, J.Z., Han, X.Q., et al., 2018b. Comprehensive investigations into low temperature oxidation of heavy crude oil. J. Petrol. Sci. Eng. 171, 835–842. https://doi.org/10.1016/j.petrol.2018.08.027.
Zhao, S., Pu, W., Peng, X., Zhang, J., Ren, H., et al., 2021. Low-temperature oxidation of heavy crude oil characterized by TG, DSC, GC-MS, and negative ion ESI FT-ICR MS. Energy 214, 119004. https://doi.org/10.1016/j.energy.2020.119004.
Zhao, S., Pu, W., Sun, B., Gu, F., Wang, L., 2019a. Comparative evaluation on the thermal behaviors and kinetics of combustion of heavy crude oil and its SARA fractions. Fuel 239, 117–125. https://doi.org/10.1016/j.fuel.2018.11.014.
Zhao, S., Pu, W., Varfolomeev, M.A., Yuan, C., Qin, S., Wang, L., et al., 2019b. Thermal behavior and kinetics of heavy crude oil during combustion by high pressure differential scanning calorimetry and accelerating rate calorimetry. J. Petrol. Sci. Eng. 106225, 181. https://doi.org/10.1016/j.petrol.2019.106225.
Zhao, S., Pu, W., Varfolomeev, M.A., Yuan, C., Rodionov, A.A., 2019c. Integrative investigation of low-temperature oxidation characteristics and mechanisms of heavy crude oil. Ind. Eng. Chem. Res. 58 (31), 14595–14602. https://doi.org/10.1021/acs.iecr.9b03346.
Zhao, S., Pu, W., Yuan, C., Peng, X., Zhang, J., Wang, L., et al., 2019d. Thermal behavior and kinetic triplets of heavy crude oil and its SARA fractions during combustion by high-pressure differential scanning calorimetry. Energy Fuels 33, 3176–3186. https://doi.org/10.1021/acs.energyfuels.9b00399.
Zheng, R., Pan, J., Chen, L., Tang, J., Liu, D., Song, Q., et al., 2018. Catalytic effects of montmorillonite on coke formation during thermal conversion of heavy oil. Energy Fuels 32, 6737–6745. https://doi.org/10.1021/acs.energyfuels.8b01157.
Zhu, Z., Liu, C., Gong, Y., Song, Y., Liu, Y., Zhao, R., et al., 2019. Integrated modeling of in-situ combustion from laboratory to field scale. SPE Western Regional Meeting, San Jose, California, 23-26 April. Society of Petroleum Engineers. https://doi.org/10.2118/195314-MS.